JACS
JOURNAL OF THE AMERICAN CHEMICAL SOCIETY

Article

pubs.acs.org/JACS

Fingerprints of Through-Bond and Through-Space Exciton and Charge π-Electron Delocalization in Linearly Extended [2.2]Paracyclophanes

José L. Zafra,[†] Agustín Molina Ontoria,[‡,§] Paula Mayorga Burrezo,[†] Miriam Peña-Alvarez,[∥] Marek Samoc,[⊥] Janusz Szeremeta,[⊥] Francisco J. Ramírez,[†] Matthew D. Lovander,[#] Christopher J. Droske,[#] Ted M. Pappenfus,[#] Luis Echegoyen,[▽] Juan T. López Navarrete,*[,†] Nazario Martín,*[,‡,§] and Juan Casado*[,†]

[†]Department of Physical Chemistry, University of Málaga, Campus de Teatinos s/n, Málaga 29071, Spain

[‡]IMDEA-Nanociencia, C/Faraday 9, Ciudad Universitaria de Cantoblanco, 28049 Madrid, Spain

[§]Department of Organic Chemistry, Faculty of Chemistry and [∥]Department of Physical Chemistry, Chemistry Faculty, University Complutense of Madrid, 28040 Madrid, Spain

[⊥]Advanced Materials Engineering and Modelling Group, Faculty of Chemistry, Wroclaw University of Science and Technology, 50370 Wroclaw, Poland

[#]Division of Science and Mathematics, University of Minnesota, Morris, Minnesota 56267, United States

[▽]Department of Chemistry, University of Texas at El Paso, El Paso, Texas 79968, United States

Supporting Information

ABSTRACT: New stilbenoid and thiophenic compounds terminally functionalized with donor−donor, acceptor−acceptor, or donor−acceptor moieties and possessing a central [2.2]paracyclophane unit have been prepared, and their properties interpreted in terms of through-bond and through space π-electron delocalization (i.e., π-conjugations). Based on photophysical data, their excited-state properties have been described with a focus on the participation of the central [2.2]paracyclophane in competition with through-bond conjugation in the side arms. To this end, two-photon and one-photon absorption and emission spectroscopy, as a function of temperature, solvent polarity, and pressure in the solid state have been recorded. Furthermore, charge delocalization through the [2.2]paracyclophane in the neutral state and in the oxidized species (radical cations, dications and radical trications) has been investigated, allowing the elucidation of the vibrational Raman fingerprint of through-space charge delocalization. Thus, a complementary approach to both "intermolecular" excitation and charge delocalizations in [2.2]paracyclophane molecules is shown which can serve as models of charge and exciton migration in organic semiconductors.

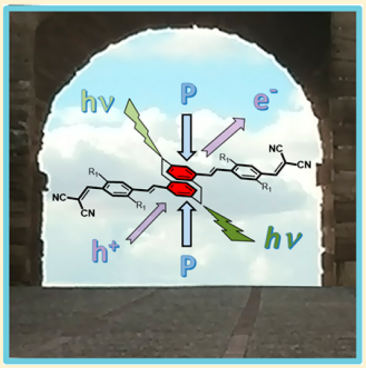

1. INTRODUCTION

The so-called "phane state" of [2.2]paracyclophanes, defined as pCp, represents an excimer-like state generated by wave function delocalization between the two sandwiched benzenes, which is promoted by the cofacial through-space (TS) coupling of the two aromatic units.[1−5] Thus, pCp[6] is a well-defined molecular model for interchromophoric exciton and charge delocalizations, a critical aspect to understand more complex unique solid-state intermolecular phenomena taking place in crystalline and in amorphous organic semiconductors. The [2.2]paracyclophane unit covalently extended with oligoparaphenylene-vinylenes[7−9] (stilbenoids) and oligothiophenes[10−12] has been reported as a way to combine through-bond (TB) and TS π-electron delocalization and conjugation in one single molecule (Scheme 1). As a result, structure−property studies with pCp-based conjugated molecules can provide significant insights to develop novel designs of molecules and polymers with enhanced optoelectronic performance.

The coupling in π-extended pCp chromophores of the two relevant perpendicularly disposed TB and TS electronic paths (Scheme 1) results in the formation of complementary states which, given the nature of their orthogonal arrangement, can compete for the stabilization of the exciton or of the charge. This provides a scenario where the optical and electronic properties can be tuned from paracyclophane-type to branch-type. For instance, the synergistic competition between TB and TS in donor−acceptor extended pCp has been exploited in photovoltaic devices. Thereby, direct donor-to-acceptor elec-

Received: December 5, 2016
Published: February 7, 2017

DOI: 10.1021/jacs.6b12520
J. Am. Chem. Soc. 2017, 139, 3095−3105

Scheme 1. (Top) The [2.2]Paracyclophane Unit, pCp, and the Relevant Electronic Through-Bond and Through-Space Effects in Conjugated Extended Systems and (Bottom) Exciton and Charge Delocalization in pCp

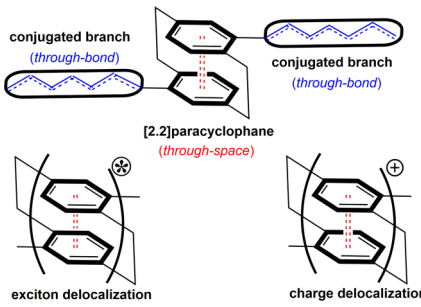

tron transfer has been shown to be effective in generating the charge separated state (radical anion and cation) by action of TB plus TS connections. However, the charge recombination kinetics is slowed down by the blockage of TS conjugation.[5] The excimer-like character of the relevant "phane" excited state has been characterized by linear optical[13] methods, two-photon absorption,[8,9,14] fluorescence,[1−7] and by nanosecond and microsecond transient absorption spectroscopies,[5,15] mainly in the seminal work of Bazan et al. The effect of charge delocalization in pCp compounds has been much less explored.

Among the many classes of pCp's substituted with conjugated arms, two different concepts have been mainly studied: (i) those with "linear" shape, or pseudopara-derivatives, where the branches are aligned in the same direction (these branches can be identical or possess a donor−acceptor configuration[16−18]); and (ii) those with a "banana" shape, or pseudo-ortho-derivatives, where the branches are disposed in 2D directions.[1,3,8] Since the interactions between TB and TS channels govern the relevant optical properties, we studied several cases of linearly substituted pCp derivatives (all compiled in Scheme 2),

Scheme 2. Chemical Structures and Abbreviation of the pCp Studied in This Work

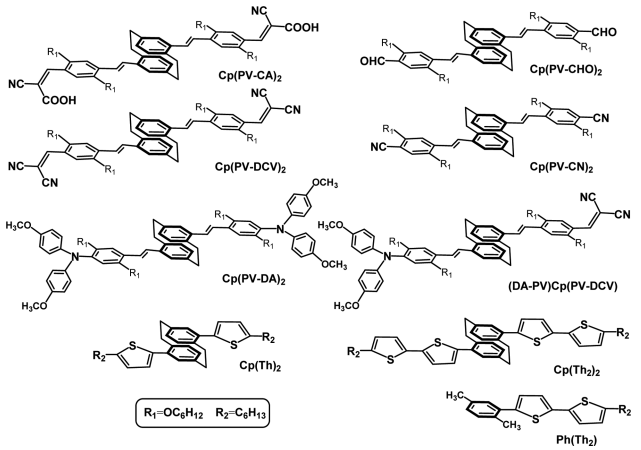

namely: (i) phenylene-vinylenes (PV, stilbene) acceptor−acceptor dyads that are substituted at the terminal positions with electron-acceptor groups of variable electron-withdrawing strength; (ii) phenylene-vinylenes (PV, stilbene) donor−donor dyads, derivatives where the pCp PV core are substituted by bisphenyl amino groups; (iii) phenylene-vinylenes (PV, stilbene) donor−acceptor dyads where the pCp PV core is substituted with a donor group at one side and an acceptor at the other; and (iv) thiophene donor−donor dyads where the stilbenoid (without donor or acceptor groups) branches are replaced by thiophenes.

This study mainly focuses on the properties governed by the phane unit with special attention on: (i) excited states which exhibit excitonic delocalization in the neutral molecules through the pCp core and (ii) oxidized species exhibiting charge delocalization between the parallel benzenes in the ground electronic state. A variety of linear absorption and photoluminescence methods have been explored in the case of the excited-state analysis, such as solvato- and thermo-chromism and pressure-dependent properties and two-photon absorption spectroscopy. To address charge delocalization in the ground electronic state, the vibrational Raman spectra in different oxidation states (radical cations, dications, and radical trications) were recorded. Quantum chemical calculations were conducted to support and understand the spectroscopic data.

2. EXPERIMENTAL AND THEORETICAL DETAILS

2.1. Synthesis. The preparation of the symmetrically functionalized donor−donor, acceptor−acceptor pCp derivatives was carried out by stepwise syntheses following well-established protocols under an inert atmosphere, summarized in Scheme 3. The starting dialdehyde **Cp(PV-CHO)$_2$** was

Scheme 3. Preparation of Stilbene-Based Donor−Donor, Acceptor−Acceptor and Donor−Acceptor Materials[a]

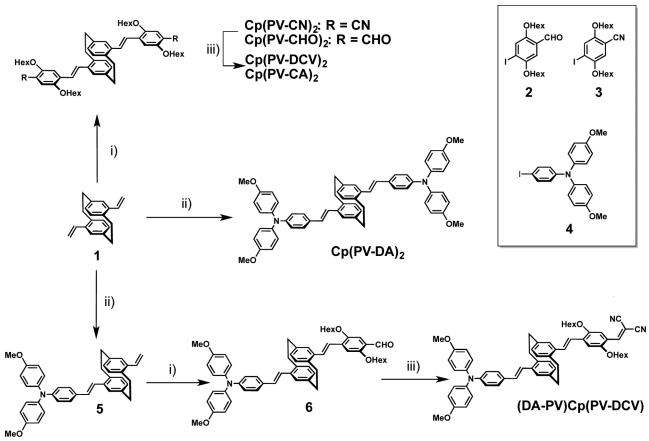

[a]Reagents and conditions: (i) Corresponding reagent **2** or **3**, $Pd(OAc)_2$, Bu_4NBr, K_2CO_3, DMF, 100 °C; (ii) **4**, $Pd(OAc)_2$, Bu_4NBr, K_2CO_3, DMF, 100 °C; (iii) corresponding reagent dicyanomethane or cyanoacetic acid, AcOH, NH_4Ac, $CHCl_3$.

obtained as previously described.[5,19] Similarly, the syntheses of the dicyano derivative **Cp(PV-CN)$_2$** and diphenylamine derivative **Cp(PV-DA)$_2$** were carried out by a 2-fold Heck Pd-catalyzed reaction between 4,16-divinyl[2.2]paracyclophane and 4-iodobenzonitrile and/or 4-iodo-*N*,*N*-bis(4-methoxyphenyl)aniline in good yields (67−75%). On the other hand, malononitrile and cyanoacetic acid were covalently connected to the dialdehyde **Cp(PV-CHO)$_2$** by a 2-fold Knoevenagel condensation, affording **Cp(PV-DCV)$_2$** and **Cp(PV-CA)$_2$** in 89% and 91% yields, respectively. The syntheses of asymmetrically substituted precursors bearing donor and acceptor moieties were performed by two consecutive Heck reactions

DOI: 10.1021/jacs.6b12520
J. Am. Chem. Soc. 2017, 139, 3095−3105

to afford compound **6** (see Scheme S1). Finally, **(DA-PV)Cp(PV-DCV)** was obtained by a Knoevenagel condensation between malononitre and monoaldehyde **6** in 83% yield. The aforementioned new compounds were spectroscopically characterized by standard techniques (FTIR, ^{1}H NMR, ^{13}C NMR, and HR-MS, see Supporting Information, Section S1). As representative spectroscopic features, all the compounds showed the corresponding signal of the ethylene bridges as three broad multiplets, integrating for 2:1:1, in the range of 2.8−3.6 ppm in the ^{1}H NMR spectra. The chemical structures of all new compounds were ascertained by HR-MS.

Previously, Collard and co-workers reported the use of a Stille coupling reaction to produce donor−donor compounds with thiophenes in place of stillbenoid branches around the pCp core.[10] However, according to the authors, this coupling method provided analytically impure products in low yield. The use of Suzuki coupling to produce similar compounds with high purity (according to combustion analyses) in moderate to good yield, as shown in Scheme 4, is reported in this study. The

Scheme 4. Preparation of Thiophene-Based Donor−Donor Materials

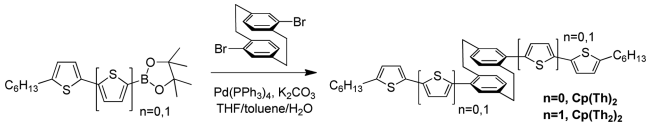

addition of hexyl-capped thienyl or bithienyl boronic esters to 4,16-dibromo[2.2]paracyclophane produced **Cp(Th)$_2$** and **Cp(Th$_2$)$_2$** in yields of 79% and 41%, respectively. The model compound, **Ph(Th$_2$)** (Scheme 2) was prepared in a similar manner using 2-bromo-*p*-xylene in place of the dibromoparacyclophane. Structures of these new compounds were confirmed by ^{1}H and ^{13}C NMR (see Schemes S2−4).

2.2. Absorption and Emission Measurements. UV−vis absorption and fluorescence spectra were recorded in a FLS920P spectrofluorometer from Edinburgh Analytical Instruments equipped with a pulsed xenon flash-lamp using the time correlated single photon counting (TCSPC) operation mode. UV−vis-NIR spectra were measured with a Cary 3000 spectrophotometer.

2.3. Raman Spectroscopy. The Raman spectra were recorded in resonance conditions either by using the 1064 or 785 nm excitations. The 1064 nm FT-Raman spectra were obtained with an FT-Raman accessory kit (FRA/106−S) using a Bruker Equinox 55 FT-IR interferometer. A continuous-wave Nd-YAG laser working at 1064 nm was employed for excitation. A germanium detector operating at liquid nitrogen temperature was used. Raman scattering radiation was collected in a back-scattering configuration with a standard spectral resolution of 4 cm^{-1}. For each spectrum, 1000−3000 scans were averaged. Raman spectra with the 785 nm excitation were collected using the 1 × 1 camera of a Bruker Senterra Raman microscope by averaging spectra during 50 min with a resolution of 3−5 cm^{-1}. A CCD camera operating at −50 °C was used.

2.4. Third-Order Nonlinear Optical (NLO) Characterization. The third-order nonlinear properties were investigated using the Z-scan technique. This technique allows to simultaneously measure both the real Re(γ) and imaginary Im(γ) parts of the cubic hyperpolarizability that are responsible for nonlinear refraction and nonlinear absorption, respectively. The nonlinear absorption data can also be presented as the two-photon absorption cross section σ_2. The measurements were performed in the wavelength range from 560 to 1000 nm using laser pulses from a Quantronix Palitra-FS optical parametric amplifier (OPA), pumped with 130 fs, 800 nm pulses at 1 kHz repetition rate from a Quantronix Integra-C Ti:sapphire regenerative amplifier. Open and closed-aperture Z-scan traces were recorded simultaneously by a pair of photodetectors, one of which was obscured by a 1 mm aperture. A detailed description of the experimental procedure can be found elsewhere.[20] The results were analyzed using the equations derived by Sheik-Bahae et al.[21]Samples of the pCp derivatives were prepared as 1% w/w chloroform solutions in 1 mm path length glass cuvettes.

2.5. Pressure-Dependent Measurements. High-pressure emission experiments were conducted in a sapphire anvil cell (SAC)[22] with a diameter culet of 360 μm and a gold gasket. The photoluminescence shift of the anvils[23,24] sapphire R1 and R2 bands was used to calibrate the pressure.[25] A no pressure transmitting medium and an air-cooled ILT argon ion laser operated at 488.0 nm were used. Emission measurements were conducted using an AvaSpec-2048-2 spectrometer with a 1200l/mm grating. Raman high-pressure measurements were conducted with the same anvils configuration using the shift of diamond chips as the pressure calibrant[26] and performed using an air-cooled argon ion laser and a Spectra-Physics solid-state laser operating at 532.0 nm. The device is equipped with a 10× Mitutoyo long working distance objective coupled to a 10× Navitar zoom system and focused onto the slit of an ISA HR460 monochromator with a grating of 600 grooves mm^{-1} and a liquid nitrogen cooled CCD detector (ISA CCD3000, 1024−256 pixels). Spectra were measured with a resolution of 2−3 cm^{-1} and calibrated with a standard neon emission lamp.

2.6. Theoretical Calculations. Quantum chemical calculations were done in the framework of the density functional theory (DFT)[27] as implemented in the Gaussian 09 package.[28] Simulations were performed in the gas-phase. The B3LYP[29] and exchange−correlational functional and the 6-31G**[30] basis set were used in all calculations. Theoretical frequencies were scaled down by a uniform scale factor of 0.96.[31] The unrestricted-B3LYP/6-31G** approach was used for the open-shell radical trication and dications. To simulate the open-shell ground-state structures of the dications, we used the broken-symmetry option with the key guess = mix keyword also with the unrestricted wave functions at the (U)B3LYP level.

3. RESULTS AND DISCUSSION

3.1. Acceptor−Acceptor Dyads. *3.1.1. Absorption Spectra and Orbital Description.* Figure 1 displays the electronic absorption spectra of the acceptor−acceptor dyads in tetrahydrofuran at 298 K. The most intense absorption of **Cp(PV-CA)$_2$** is at 450 nm which at the TD/DFT/6-31G** level (see Figures 1 and S1 for the theoretical spectra) corresponds to the $S_0 \rightarrow S_3$ excitation at 471 nm (oscillator strength, f = 2.07) described as the sum of the H-1 → L and H → L one-electron promotions. These orbitals in Figure 1 (Figure S2 and Table S1) are centered in the branches with the two benzenes of the PV units participating in the TB conjugation. No interactions between the two benzenes of the paracyclophane unit are noticeable. There is a medium intensity band at 396 nm in the spectrum, predicted as the $S_0 \rightarrow S_7$ excitation and calculated at 396 nm (f = 0.22), arising

DOI: 10.1021/jacs.6b12520
J. Am. Chem. Soc. 2017, 139, 3095−3105

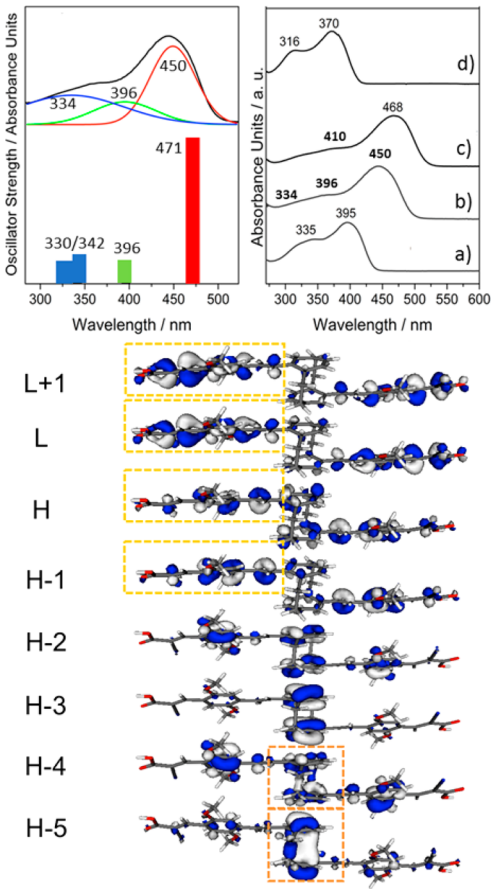

Figure 1. Top left: Absorption spectrum of **Cp(PV-CA)$_2$** with its pertinent deconvolutions together with the TD/DFT theoretical excitations (as bars). Top right: absorption spectra of the four compounds in THF at 298 K: (a) **Cp(PV-CHO)$_2$**, (b) **Cp(PV-CA)$_2$**, (c) **Cp(PV-DCV)$_2$**, and (d) **Cp(PV-CN)$_2$**. Bottom: Frontier molecular orbitals topologies of **Cp(PV-CA)$_2$**. Yellow and orange boxes highlight the main orbital π-distribution.

from multielectron promotions between the H-4 → L and H-2 → L + 1 orbitals. The third band at 334 nm is related to two theoretical excitations: the first one, the $S_0 \rightarrow S_{11}$ excitation, calculated at 342 nm ($f = 0.21$), due to an H-5 → L promotion, and the second one, due to the $S_0 \rightarrow S_{13}$ excitation, calculated at 330 nm ($f = 0.19$), arising from a H-1 → L + 2 promotion. Interestingly, these two last excitations involve orbitals, H-4 and H-5, where inter-ring cofacial wave function delocalization within the pCp, or TS delocalization, is feasible (Figure 1).

Calculations on the model compound consisting only of the isolated arm (PV-CA unit), or donor–acceptor TB conjugated compound, show that the lowest energy lying electronic transition is due to the $S_0 \rightarrow S_1$ excitation, which is mostly associated with a HOMO → LUMO promotion (see Figure S3 and Table S2). In this PV-CA structure, the HOMO wave function is mainly placed on the donor PV unit, whereas the LUMO is mostly located on the cyano-carboxylic-vinylene moiety. Thus, this excitation promotes an electron density shift, or CT character. In contrast, in the **Cp(PV-CA)$_2$** dyad, the lowest energy excitations (i.e., the $S_0 \rightarrow S_1$ and $S_0 \rightarrow S_2$) are forbidden transitions (oscillator strength, $f = 0$) and thus inactive in the one-photon absorption spectrum. This means that in **Cp(PV-CA)$_2$**, a significant blue-shift of the strongest observed UV–vis band takes place, compared with that of the individual donor–acceptor arm (from $S_0 \rightarrow S_1$ in the PV-CA arm to the $S_0 \rightarrow S_3$ in the **Cp(PV-CA)$_2$** dyad).

For the four compounds, the strongest absorption bands move to the red 445 → 468 and 354 → 370 nm on **Cp(PV-CA)$_2$**→ **Cp (PV-DCV)$_2$**, given the strengthening of the acceptor character upon replacing the carboxylic group by another cyano. The main electronic absorption bands of the UV–vis spectra of the cyano and aldehyde substituted dyads [i.e., **Cp(PV-CN)$_2$** and **Cp(PV-CHO)$_2$**] blue-shift considerably, compared to the other two derivatives, in agreement with the diminished electron-withdrawing strength of these terminal groups.

3.1.2. Emission Fluorescence Spectra. The photophysical properties reported for pCp-based conjugated molecules have been interpreted in terms of the relative energy location of the "phane" TS excimer-like state (E_{TS}) relative to that of the "arms" TB state (E_{TB}) in Scheme 5.

Scheme 5. Relative Disposition of the Relevant Excited States.[a] Emissions from (A) the TB State in Large Conjugated Arms, (B) the TS State in Short Conjugated Arms, and (C) the TB State in Coplanar Donor–Acceptor Arms; (D) Mixed Emission from a TS State Extended Partially on the Arms in a TICT State; (E) the Case of Dual Emission; and (F) Emission from a "Compressed" Excited State

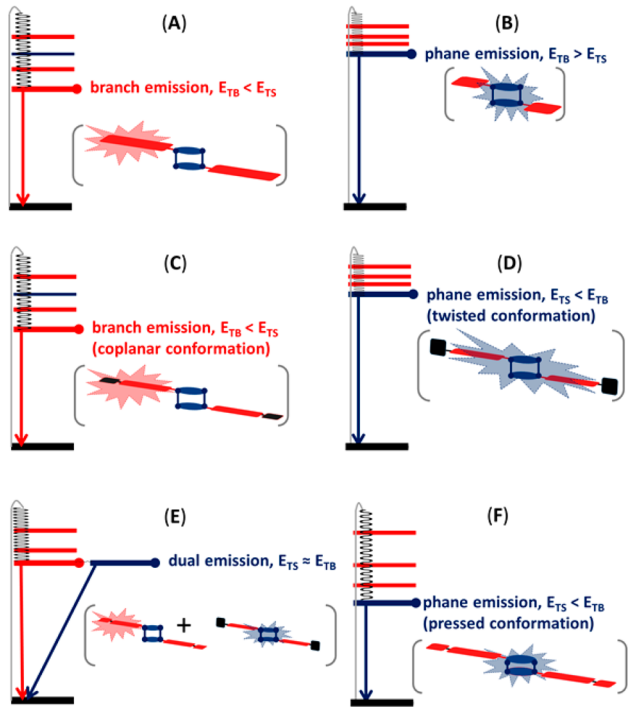

[a]Red: TB states on the branches; blue: TS state in the pCp unit.

For long conjugated arms, the energy of the TB state is lower than that of the "phane" TS state (case A in Scheme 5, $E_{TB} < E_{TS}$), and both absorptions and emissions are dominated by the TB delocalization in the arms. Conversely, in the case of short conjugated arms (case B in Scheme 5, $E_{TB} > E_{TS}$), the photophysical properties are dictated by the TS "phane" state. According to the description above, in the case of **Cp(PV-CA)$_2$**, the molecular orbitals containing the TS interaction (H-4, H-5) contribute to higher energy excited states compared to

DOI: 10.1021/jacs.6b12520
J. Am. Chem. Soc. 2017, 139, 3095–3105

the states related to the TB orbitals (H, H-1, etc.). This means that, despite the rather small stilbenoid conjugated arms (case C in Scheme 5, $E_{TB} < E_{TS}$), the inclusion of acceptor moieties enables a substantial decrease of the E_{TB} energy compared to E_{TS} in these substituted pCp.

Figure 2 displays the excitation and emission spectra of **Cp(PV-CA)$_2$** and **Cp(PV-DCV)$_2$** in a polar solvent, DMF.

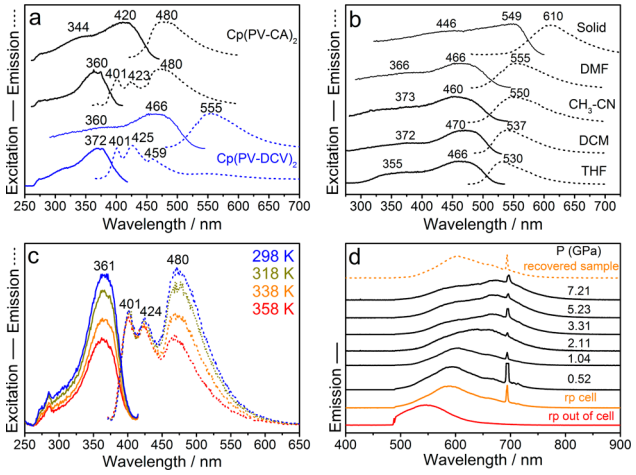

Figure 2. (a) Excitation/emission spectra of **Cp(PV-CA)$_2$** and **Cp(PV-DCV)$_2$** in DMF at 298 K. The high/lower energy excitation spectra in blue (black) are recorded with the emission at 425 (420)/555 (487) nm, whereas the high/lower energy emission spectra are taken by exciting at 360 (350)/472 (420) nm. (b) Excitation/emission spectra of **Cp(PV-DCV)$_2$** recorded in solid state (red) and in different solvents (black). (c) Excitation/emission spectra of **Cp(PV-CA)$_2$** as a function of temperature. (d) Emission spectra of **Cp(PV-DCV)$_2$** in solid state as a function of applied pressure.

Excitation of the strongest absorption band at 420 nm for **Cp(PV-CA)$_2$** gives rise to a broad featureless emission at 480 nm. However, by exciting at 350 nm, a dual emission is recorded, which consists of a higher energy emission component with vibronic structure between 400 and 430 nm, followed by a second emission at 480 nm, identical to the one described by exciting the lowest absorption band. According to the TD-DFT excited-state calculations, in the first experiment, the $S_0 \rightarrow S_3$ excitation is promoted, which is a TB excited state placed in the conjugated arms. It relaxes by internal conversion to the lowest energy S_1 excited state, also confined in the conjugated arms, from which it emits light (case A in Scheme 5). This $S_1 \rightarrow S_0$ emission is weak (the $S_0 \rightarrow S_1$ absorption is inactive) and featureless given its charge-transfer character (HOMO → LUMO). By exciting the $S_0 \rightarrow S_7$ "phane state" at 360 nm, another high-energy vibronically resolved band, which might be ascribed to an emission from a mixed state involving the pCp and also, partially, the conjugated arms (excluding the acceptor groups) (case D in Scheme 5), is observed. Since the TB and TS states are orthogonally decoupled, this mixed excited state can either emit (emerging the high-energy component of the emission) or be depopulated by internal conversion to the S_1 charge-transfer excited state (resulting in the second lowest energy emission). In order to justify why the electronic contributions of the acceptor groups are removed in this mixed excited state, the formation of TICT states can be invoked. In conjugated donor–acceptor dyes, twisted intramolecular charge-transfer states (TICT) fully decouple the donor–acceptor interaction and consist of conformations, as represented in case D of Scheme 5, where the acceptor groups acquire a perpendicular disposition relative to the stilbenoid arms. In this way the acceptor groups are fully removed from any participation in the emission as a result of the interaction with the polar solvent.[32] This is likely the case in the DMF polar solvent, where dual emission emerges due to the presence in solution of both twisted and coplanar conformers (case E in Scheme 5). A very similar situation is found for **Cp(PV-DCV)$_2$**, where exciting the "phane" state produces a vibronically resolved emission at the same wavelength as the **Cp(PV-CA)$_2$**, corroborating that it comes from the common pCp phenylene-vinylene spacer (TICT state). In this case, the lowest energy coplanar charge-transfer emission is resolved at 555 nm, red-shifted relative to the analogue emission at 480 nm in **Cp(PV-CA)$_2$**. These TICT states are analogue to the TICTOID systems in which steric hindrance between the donor/acceptor moieties and the bridge forces them to a perpendicular disposition, which, in contrast with our cases, further imparts zwitterionic character and large NLO response. On the other hand, these TICT states are not analogue to those described in donor–π–donor systems.[33]

To further understand the excited-state distribution resulting from the pCp insertion, two new compounds, where thiophene units replace the stilbene branches, were prepared. The two new compounds possess one (**Cp(Th)$_2$**) or two thiophenes (**Cp(Th$_2$)$_2$**) in each branch terminated with hexyl groups. In Figure 3 the absorption and emission spectra of the two

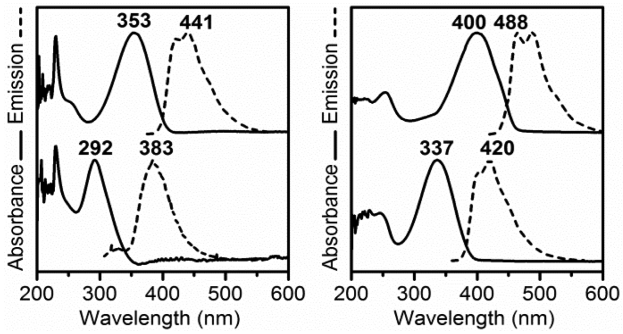

Figure 3. UV–vis absorption and emission spectra in dichloromethane of **Cp(Th)$_2$** (bottom left), **Cp(Th$_2$)$_2$** (top left), **Ph-Th$_2$** (bottom right), and **DMQtT** (top right).

compounds together with the reference (i.e., the isolated arm) compound **Ph-Th$_2$** are shown. The absorption maximum is at 292 nm for **Cp(Th)$_2$** and red-shifts to 353 nm for **Cp(Th$_2$)$_2$**. These spectra are in excellent agreement with methyl terminated homologues previously published by Collard.[10] The unique effect of the insertion of the pCp, or of the TS conjugation, is seen by comparing the results for the **Ph-Th$_2$** reference compound with those of **Cp(Th$_2$)$_2$** and with dimethylquaterthiophene, **DMQtT** (i.e., the parent compound without the central pCp unit). The reference compound displays an absorption maximum at 337 nm, whereas **DMQtT** and **Cp(Th$_2$)$_2$** display maxima at 400 and 353 nm, respectively. This influence is also seen in the wavelength maxima of the emission spectra, as these are detected at 383 nm for **Cp(Th)$_2$**, at 420 nm for **Ph-Th$_2$**, at 488 nm for **DMQtT**, and at 441 nm in **Cp(Th$_2$)$_2$**. The most noticeable aspect of the emission spectra of **Cp(Th$_2$)$_2$** and **Ph-Th$_2$** is the vibronic structure, while the emission spectrum of **Cp(Th)$_2$** is featureless. This clearly indicates the participation of a pure "phane" excited state (in

DOI: 10.1021/jacs.6b12520
J. Am. Chem. Soc. 2017, 139, 3095–3105

contrast with the mixed character of the stilbenoid cases above) in the emission of **Cp(Th)$_2$**, while this phane effect is deactivated for the branch centered emission of **Cp(Th$_2$)$_2$**. Consequently, whereas for **Cp(Th)$_2$** the emission is net for the TS "phane" state, for **Cp(Th$_2$)$_2$** it mainly emerges from the TB state. Additionally, in the stilbenoid compounds the emission is complicated by the presence of the TICT states and by the mixing of the pCp and the phenylene-vinylene spacer states.

*3.1.3. Solvent, Temperature, And Pressure Effects on the Absorption and Fluorescence Spectra of **Cp(PV-CA)$_2$** and **Cp(PV-DCV)$_2$**.* To further confirm these interpretations, photophysical measurements in an apolar solvent, dichloromethane (Figure 2, top right), where no double emission is observed, were conducted. The weak polar character of this solvent deactivates the TICT effect by which the acceptors remain coupled with the conjugated PV unit in the TB path. Furthermore, fluorescence emission spectra as a function of the temperature are shown in Figure 2 (bottom left) for **Cp(PV-CA)$_2$**. It can be observed that by increasing the temperature, the lowest-lying energy CT emission declines in intensity in favor of the mixed TICT state. This effect can be explained on the basis of increased conformational mobility at high temperatures, around the single bond connecting the phenylene-vinylene unit to the acceptor, which directly promotes the TICT effect and its vibronically resolved emission.

Solvent and temperature modify the acceptor molecular environment, hence, in order to get further insights about the central "phane" unit, a pressure-dependent emission experiment in the solid state was conducted, see Figure 2.[34] The face-to-face interaction in the pCp core is expected to change by slightly reducing the interbenzene distance. Owing to the large sensitivity of the energy of the excimer-like "phane" state to this interannular distance, a modification of the emission features was expected. In the solid state at ambient pressure, upon excitation of the 350 nm excimer-like "phane" absorption, no double emission was observed. Furthermore, the TB emission of the branches appears further red-shifted at 610 nm compared to the solution spectrum. However, at high pressure, up to 1.95 GPa, the TB charge-transfer emission at 610 nm develops a low-energy feature at 680 nm that becomes the most intense emission component at 7.0 GPa. For all pressures analyzed at room temperature, the 610 and 680 nm components coexist, whereas the original spectrum is recovered upon removing pressure. These results can be explained considering that the formation of a TICT excited state is highly impeded in the solid state due to largely restricted conformational freedom. The application of pressure likely results in a compression of the pCp unit, increasing the $\pi-\pi$ cofacial benzene interaction that stabilizes the excimer-like "phane" state (see case F in Scheme 5), which would appear at lower energies, partially overlapped with the low-energy TB band and, as a result, contributing to the 680 nm component of the emission under pressure.

3.1.4. Two-Photon Absorption Properties. Two-photon absorption cross sections (σ_2(GM)) for the four stilbenoid compounds were measured by means of the Z-scan technique, using a tunable femtosecond laser system. Table 1 summarizes the data from the third-order nonlinear measurements at wavelengths corresponding to σ_2 peaks, and Figure 4 displays the two-photon absorption cross-section spectra. In order to properly analyze the data for compounds having different molecular masses, the merit factor, which is the two-photon absorption cross-section divided by the molar mass (σ_2/M), is also presented. This also allows for comparison between

Table 1. Third-Order NLO Data Determined with the Z-Scan Technique

sample	λ_{max} [nm]	Re(γ) [10^{36}esu]	Im(γ) [10^{-36}esu]	σ_2 [GM]	σ_2/M [GM mol/g]
Cp(PV-CHO)$_2$	625	−230	200	82	0.094
	850	62	160	36	0.041
Cp(PV-CA)$_2$	675	−1080	730	255	0.254
	825	−670	1050	247	0.246
Cp(PV-DCV)$_2$	650	−670	610	233	0.241
	825	−240	1440	340	0.352
Cp(PV-CN)$_2$	600	−530	102	45	0.052
	900	−72	74	15	0.017

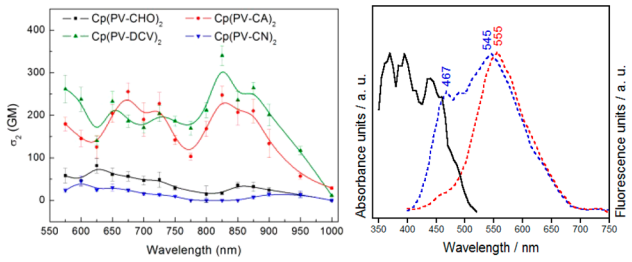

Figure 4. Left: Two-photon absorption spectra recorded with the Z-scan techniques. Right: Two-photon-induced up-conversion fluorescence analysis for compound **Cp(PV-DCV)$_2$** in DMF.

various types of nonlinear materials (small molecules, polymers, branched dendrimers, or nanoparticles).[35]

The linear absorption/emission properties show that the TB and TS excited states are affected by several environmental and molecular changes. The existence of two identical donor–acceptor branches connected through the pCp unit gives rise to an opposite arrangement of the local dipole moments on each branch, leading to the appearance of excitations which might be prone to two-photon absorption activity.[8,9,14] Compounds **Cp(PV-CA)$_2$** and **Cp(PV-DCV)$_2$** show the highest σ_2(GM) TPA values, much higher than those of **Cp(PV-CHO)$_2$** and **Cp(PV-CN)$_2$** given their smaller π-spaces and electron-withdrawing strengths (both weaken the charge-transfer character). It is interesting to inspect the TPA bands in terms of TD-DFT calculations by assuming that those excitations predicted with zero or vanishing oscillator strength in the one-photon absorption spectrum are caused by "dipolar symmetric transitions", which is actually the condition for two-photon absorption bands to be active. Two main TPA peaks are observed at 825 and 680 nm. The TPA band maximum at 825 nm, which is accompanied by a peak around 880 nm, can be associated with the $S_0 \rightarrow S_2$ and $S_0 \rightarrow S_1$ excitations, respectively, theoretically predicted at 472/480 nm (944/960 nm). There are two other less intense TPA bands around 680 nm which might be correlated with the one-photon silent excitations, $S_0 \rightarrow S_4$, $S_0 \rightarrow S_5$, and $S_0 \rightarrow S_6$, predicted theoretically at 446, 404, and 399 nm, respectively (Table S1).

To complete the TPA study in terms of the distributions of excited states, two-photon-induced up-conversion fluorescence analysis for compound **Cp(PV-DCV)$_2$**, as a representative example, was conducted. The spectra are shown in Figure 4. By exciting at the longest wavelength (900 nm, TPA state at 450 nm), only one fluorescence emission peak at 555 nm was observed, in line with the excitation of the lowest energy lying TPA active excited states of the branches ($S_0 \rightarrow S_1$ and $S_0 \rightarrow S_2$). By exciting at shorter wavelengths, between 850 and 750

DOI: 10.1021/jacs.6b12520
J. Am. Chem. Soc. 2017, 139, 3095–3105

nm, two fluorescence peaks with maxima at 467 and 545 nm are observed, in agreement with the excitation of the higher energy TPA active excited state ($S_0 \rightarrow S_4/S_5/S_6$) with increasing participation of "phane" states. Figure 4 also shows the TPA excitation spectra that corroborate the assignments of the relevant TPA absorptions observed between the one-photon absorption bands.

3.1.5. Raman Spectroscopic Properties. The discussion above mainly concerns the energy position and activity of the excited states arising from TB and TS conjugation, a critical aspect to correctly design the channel for energy migration in molecules. In order to complete the characterization of pCp molecules, the conjugation properties in the ground electronic state were addressed by means of Raman spectroscopy, a technique that provides the frequencies associated with vibrational normal modes involved in the C=C/C−C conjugation paths.[36] Figure 5 displays the Raman spectra of

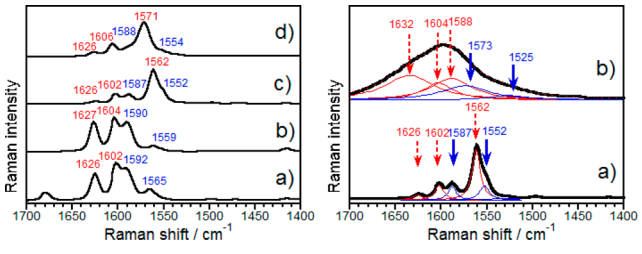

Figure 5. Left: FT-Raman spectra of the four compounds in solid state: (a) **Cp(PV-CHO)$_2$**, (b) **Cp(PV-CN)$_2$**, (c) **Cp(PV-DCV)$_2$**, and (d) **Cp(PV-CA)$_2$**. Right: Raman spectra of **Cp(PV-DCV)$_2$** in solid state at (a) room pressure and (b) 8 GPa. Lorentzian deconvolutions are shown in colors.

the acceptor−acceptor dyads. See Figure S4 for the theoretical spectrum of **Cp(PV-CA)$_2$**, where the vibrational normal modes used to assign the bands are also shown.

The band at 1626 cm^{-1} corresponds to a C=C stretching vibration of the internal vinylene bond [i.e., ν_{int}(C=C)] which connects to the pCp; the band at 1602 cm^{-1} arises from a CC stretching vibration of the PV benzene rings (i.e., ν_{TB}(CC), in the TB conjugation path), whereas the band at 1587 cm^{-1} corresponds to a CC stretching mode of the benzenes in the pCp unit [i.e., ν_{1pCp}(CC)]. A second band arising from the pCp fragment is at 1552 cm^{-1}, assigned to an analogue CC stretching mode [i.e., ν_{2pCp}(CC)]. The most intense Raman band is at 1562 cm^{-1} and results from a C=C stretching vibration of the external double bond [i.e., ν_{ext}(C=C)] connected to the acceptors units. This assignment agrees with that reported for the pCp compound which describes their relevant CC stretching modes in this region at 1599 and 1559 cm^{-1}, respectively.[34]

Based on this description of the vibrational Raman spectrum in terms of ground electronic state frequencies, their evolution in the series is possible. The two ν_{pCp}(CC) bands at 1592/1565 cm^{-1} for **Cp(PV-CHO)$_2$**, 1590/1559 cm^{-1} for **Cp(PV-CN)$_2$**, 1587/1552 cm^{-1} for **Cp(PV-DCV)$_2$**, and 1588/1554 cm^{-1} for **Cp(PV-CA)$_2$** indicate changes of the pCp Raman bands due to the external acceptor groups in the ground electronic state. Generally speaking, a frequency downshift of the vibrational modes associated with CC stretching of the aromatic benzenes reveals the transformation of the benzoaromatic-like structure into a benzoquinoidal-like one.[36] Comparing **Cp(PV-CHO)$_2$** and **Cp(PV-DCV)$_2$**, a larger ν_{pCp}(CC) frequency downshift is detected, resulting from the stronger electron-withdrawing effect of the dicyanovinyls compared with the aldehyde derivative along the TB path. The Raman frequency behavior of the ν_{TB}(CC) benzene/ν_{int}(C=C) vinylene bands is 1602/1626 cm^{-1} for **Cp(PV-CHO)$_2$**, 1604/1627 cm^{-1} for **Cp(PV-CN)$_2$**, 1602/1626 cm^{-1} for **Cp(PV- DCV)$_2$**, and 1606/1626 cm^{-1} for **Cp(PV-CA)$_2$**. These show changes toward a more TB conjugated situation in the cases with stronger acceptors. From these data, changes associated with TS conjugation cannot be deduced.

Micro-Raman spectroscopy allows monitoring frequency changes under pressure in the solid state. Pressure-dependent Raman experiments were conducted (shown in Figure 5) to follow TS conjugation changes in the pCp core. The first noticeable pressure effect in the Raman spectra is an overall spectral broadening, which is a consequence of the increment of intermolecular interactions (going from the absolute minimum along the repulsive branch of the ground electronic state potential energy surface with pressure). As a result, frequencies experience a general upshift. Based on the presence of five bands in the spectrum of **Cp(PV-DCV)$_2$** at room pressure (RP), the broad Raman feature at 1530−1600 cm^{-1} was deconvoluted into five Lorentzian components (Figure 5, fit of 0.99), which emerge at: 1632 cm^{-1} (i.e., 1626 cm^{-1} at RP), at 1604 cm^{-1} (i.e., 1602 cm^{-1} at RP), at 1588 cm^{-1} (i.e., 1562 cm^{-1} at RP), at 1573 cm^{-1} (i.e., 1587 cm^{-1} at RP), and finally at 1525 cm^{-1} (i.e., 1552 cm^{-1} at RP). Two clearly different behaviors are observed: (i) that of the 1632/1604/1588 cm^{-1} bands with small to moderate upshifts compared with frequencies at RP and (ii) that of the 1573/1525 cm^{-1} bands which show downshifts. The first three bands are due to vibrational modes on the arms, and the upshifts are caused by the increment of intermolecular interactions, however, the second pair of bands own to the pCp units, which conversely downshift upon application of pressure. Application of pressure compresses the pCp structure, resulting in a decrease of the interbenzene distance and, therefore, an increase of the TS π-delocalization. Consequently, TS delocalization might displace π-electron density from the benzene ring to the interannular region and result in the Raman downshifts.

3.2. Donor−Donor Dyad. *3.2.1. Ground Electronic-State Properties.* In the donor−donor derivatives, the vinyl−acceptor groups have been substituted by donor amino-phenyl moieties. The insertion of the nitrogens in diarylamino groups enhances the electron-donor character of the molecules and their ease of oxidation.[37,38] Therefore, these donor−donor molecules allow the analysis of the TB/TS conjugation properties of oxidized species through the pCp unit.

Figure 6 shows the theoretical Raman spectra of the pCp unit alone, where the two arms in the studied model compound have been replaced by methyls. The Raman spectrum of the neutral model displays the two characteristic Raman bands at 1590 and 1552 cm^{-1} already discussed as exclusively resulting from this pCp part. In the radical cation state, the theoretical Raman spectrum features a strong band at 1441 cm^{-1} which is accompanied by medium intensity bands at 1456 and 1416 cm^{-1}, representative of the vibrational fingerprint of the structure ("phane state" in Scheme 1). The positive charge is delocalized between the two benzenes and, as a result, displays an interbenzene distance smaller than in the neutral case, 3.050 →2.942 Å, according to B3LYP/6-31G* calculations.

A diphenylamino stilbene paracyclophane derivative (**Cp-(PV-DA)$_2$**) was prepared for the study of the oxidized species.

DOI: 10.1021/jacs.6b12520
J. Am. Chem. Soc. 2017, 139, 3095−3105

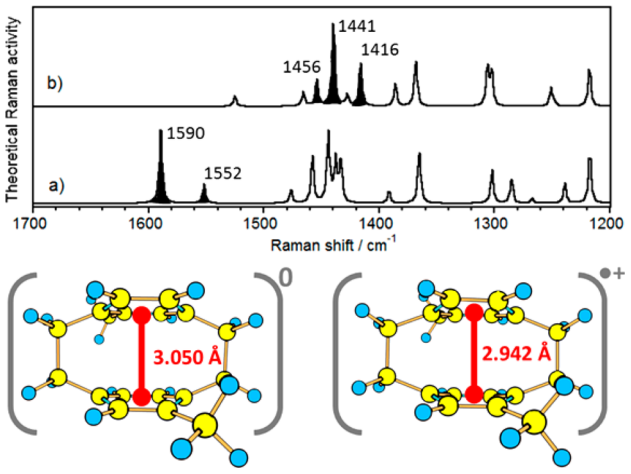

Figure 6. Top: (U)B3LYP/6-31G* theoretical Raman spectra of the dimethyl pCp unit in the neutral (a) and radical cation (b) states. Bottom: Optimized geometries with the interbenzene average distances.

Cyclic voltammetry of **Cp(PV-DA)$_2$** shows two processes: one at +0.56 V involving two electrons and another at 1.10 V which involves only one electron (see cyclic voltammogram in Figure 7 insert and Figure S5 and Table S3). It is straightforward to

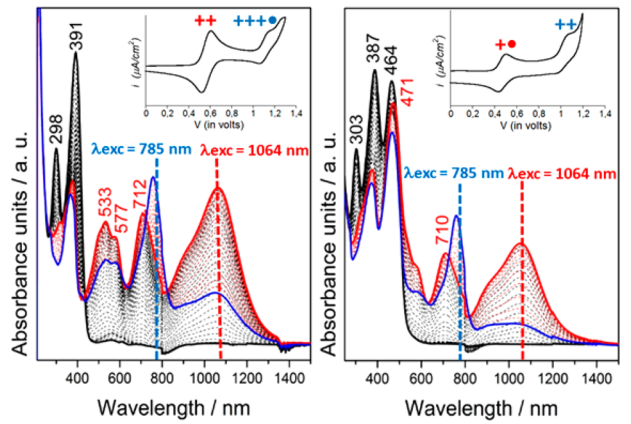

Figure 7. UV−vis-NIR spectroelectrochemistry of **Cp(PV-DA)$_2$** (left) and of (PV-**DA**)**Cp**(**PV-DCV**) (right). Dashed bars show the wavelength of the laser excitation used in the Raman experiments. The inserts correspond to the cyclic voltammetry of each compound in the anodic branch showing the formation of different polycationic states.

assign the first event to the formation of a bis(radical cation) (i.e., dication) or of a radical cation on each arm, followed by the oxidation of the central part of the molecule or radical trication mostly localized on the pCp center. Figure 7 shows the UV−vis-NIR spectra obtained upon *in situ* electrochemical oxidations of **Cp(PV-DA)$_2$**. Two different spectra are obtained, one after the disappearance of the neutral species and formation of the dication and a second spectrum upon oxidation to the radical trication. The spectrum of the dication consists of three main bands at 533(577), 712, and 1062 nm, a multiband spectroscopic pattern typical of open-shell radical cations of π-conjugated molecules.[39] This dicationic species can be viewed as an acceptor−acceptor dyad (Scheme 5) where, in fact, the structured band at 500−570 nm can be correlated with, for instance, that at 468 nm for **Cp(PV-DCV)$_2$**. Further oxidation of this species gives rise to a clear distinctive electronic absorption spectrum dominated by one band at 755 nm that results from the radical trication.

Figure 8 displays the Raman spectra of **Cp(PV-DA)$_2$** donor−donor dyads in the three relevant oxidation states. The

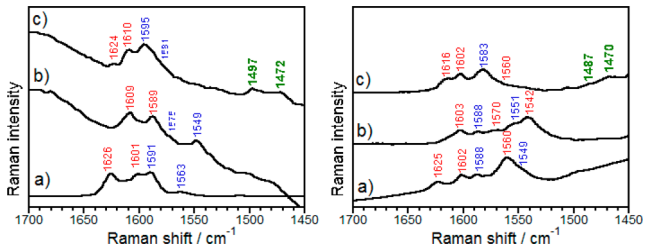

Figure 8. Left: Raman spectra of (a) neutral, (b) dication (1064 nm), and (c) radical trication (785 nm) of **Cp(PV-DA)$_2$**. Right: Raman spectra of the (a) neutral, (b) radical cation (1064 nm), and (c) dication (785 nm) of (**PV-DA**)**Cp**(**PV-DCV**). In parentheses the excitation wavelength used in the Raman experiment (see Figure 7).

spectrum of the neutral species features the presence of four bands due to the ν_{int}(C=C) at 1626 cm^{-1}, the ν_{TB}(CC) benzene at 1601 cm^{-1} and the two ν_{pCp}(CC) bands at 1591/1563 cm^{-1}.

Formation of the dication from neutral **Cp(PV-DA)$_2$** gives rise to a Raman spectrum that exhibits a downshift of the frequencies of the four neutral bands in Figure 8, as a consequence of the weakening of the vinylene bond and of the quinoidization of the benzenes. Further oxidation of this dication gives way to the radical trication, which, in contrast with the frequency behavior of the neutral → dication, displays a general frequency upshift. In addition, two new medium intensity bands appear in the Raman spectrum of the radical trication at 1497/1472 cm^{-1}. The Raman spectra of the dication and radical trication were recorded in resonance conditions with the characteristic electronic absorptions of each species, as shown in Figure 7. The dication was recorded with the 1064 nm Raman excitation line in resonance with the absorption band with maximum at 1062 nm. On the other hand, the radical trication species was obtained with the 785 nm Raman excitation line in resonance with the absorption band with maximum at 755 nm. The radical cation and dication of (**PV-DA**)**Cp**(**PV-DCV**) were similarly generated and studied, as shown in Figure 7, and are discussed in the next section.

Scheme 6 displays the main resonant forms associated with the different oxidized species of **Cp(PV-DA)$_2$**, that might justify

Scheme 6. Resonant Forms Stabilizing the Charged Species of Cp(PV-DA)$_2$ (left) and of (PV-DA)Cp(PV-DCV) (right)

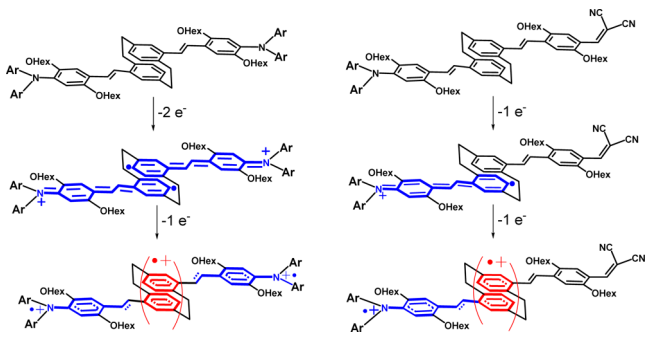

DOI: 10.1021/jacs.6b12520
J. Am. Chem. Soc. 2017, 139, 3095−3105

the Raman frequency changes. In the dication, the structural transformation spreads over the whole branch, forming quinoidal structures in the benzenes and conferring the vinylene a more single bond character. For the trication, the charge is extracted mainly from the central pCp, while the existing positive charges of the dication are fully pushed toward the outermost nitrogens for which the benzenes are forced to change their quinoidal structure toward a more aromatic shape, such as shown in Scheme 6. The new Raman bands of the radical trication at 1497/1472 cm^{-1}, therefore, might be related to the formation of a charged "phane" state with charge delocalization within the two cofacial benzenes.

These Raman bands are in good agreement with the Raman spectrum predicted for the radical cation of the dimethyl pCp unit, which supports the presence of charge delocalization in the radical trication of **Cp(PV-DA)$_2$**, and of the participation of the "phane state" in the stabilization of the charge.

3.3. Donor−Acceptor Dyad. The aryl-amino-donor and dicyano-vinyl-acceptor substituted paracyclophane compound **(PV-DA)Cp(PV-DCV)** shows a one-electron oxidation at +0.46 V, associated with the formation of a radical cation, followed by a second one-electron oxidation at +1.03 V, corresponding to the stabilization of a dication (see cyclic voltammogram in Figure 7 insert and Figure S5 and Table S3). The correlation between the formation of the dication of **Cp(PV-DA)$_2$** and of the radical cation of **(PV-DA)Cp(PV-DCV)** is straightforward, as both species stabilize one positive charge in the diphenylamino arm. On the other hand, the radical trication and dication, respectively, correspond to charge extracted from the central pCp unit. Figure 7 shows the spectroelectrochemical UV−vis-NIR spectra of **(PV-DA)Cp-(PV-DCV)** where the formation of two distinctive spectra emerging progressively from the radical cation and dication species is noticed. The radical cation is characterized by three bands 534/585, 710, and 1047 nm [i.e., correlate with the bands of the bis(radical cation) of **Cp(PV-DA)$_2$**]. Oxidation of the radical cation of **(PV-DA)Cp(PV-DCV)** leads to the formation of the dication species exhibiting one main band at 757 nm [i.e., correlated with the band at 755 nm assigned in the radical trication of **Cp(PV-DA)$_2$**].

Figure 8 also displays the Raman spectra of the oxidized species of **(PV-DA)Cp(PV-DCV)**. The Raman spectrum of the neutral contains the Raman bands associated with the ν_{int}(C═C)/ν_{ext}(C═C) at 1625/1560 cm^{-1}, the 1602 cm^{-1} band of the benzene ν_{TB}(CC), and the ν_{pCp}(CC) features at 1588/1549 cm^{-1}. Oxidation, such as in the case of **Cp(PV-DA)$_2$**, produces an overall frequency downshift which is ascribed to the formation of the radical cation placed and delocalized on the bis(aryl)amino stilbene unit, producing the quinoidization of the benzene and the transformation of the vinylene. Further oxidation of this radical cation to the dication leads to a similar behavior as that found for the radical trication of **Cp(PV-DA)$_2$**, consistent with an overall frequency upshift of these bands due to the mitigation of the quinoidal structures. The presence of an acceptor branch on one side, and of a radical cation on the other, forces the second electron extraction from the pCp unit, as shown in Scheme 6. The new bands for the dication at 1487/1470 cm^{-1} are, therefore, the characteristic vibrational signature of the "phane state", as described for the radical trication of **Cp(PV-DA)**.

Interestingly, the Raman spectrum of neutral **Cp(PV-DCV)$_2$** as a function of pressure, discussed in Section 3.1.5, shows a significant frequency downshift for the pCp bands (1587 → 1573 cm^{-1} and 1552 →1525 cm^{-1}). This is also consistent with the strong downshifts from ≈1550 cm^{-1} to 1470 cm^{-1} for the new bands observed for the radical trication and dication of **Cp(PV-DA)$_2$** and **(PV-DA)Cp(PV-DCV)**, respectively. In the former case, the charge delocalization between the two sandwiched benzenes is induced by pressure ,and in the oxidized species, the driving force is the stabilization of the positive charge by delocalization. Obviously, the latter effect results in a much stronger alteration of the interbenzene distance, and, therefore, it leads to a larger impact on the vibrational frequencies.

4. CONCLUSIONS

Intermolecular exciton and charge delocalization is an important topic in organic electronics, as it is at the origin of the energy and charge transport of semiconductor substrates. In order to better understand these complex processes, molecules with well-defined and precise structures and conformations are required to establish reliable structure−properties relationships. Here, the pCp unit, which has a face-to-face blocked conformation of two benzenes separated by ≈3 Å, that mimics the effect of TS delocalization, has been chosen. Several new pCp derivatives were synthesized and studied, possessing stilbene moieties, further substituted with donors and acceptors in several structures, and also containing thiophene derivatives replacing the stilbenoid bridges.

The detection of dual fluorescence allowed obtaining insights of the excited state ordering, which is responsible for the different emission properties measured. The extended conjugation of the linear arms is the reason why emissions are pushed far from the pCp, while limited conjugation of the arms is an efficient way for the sandwiched structure to be involved in the emissions. The excited states were analyzed by using one- and two-photon absorption properties which allow to characterize the bright and dark excited states with and without pCp participation.

In a different spectroscopic approach, using Raman spectroscopy for the study of the ground electronic-state properties, the vibrational Raman fingerprints of charge delocalization in the benzene−benzene interface were obtained. By conducting pressure-dependent Raman measurements, the interbenzene distance was partially modified, as evidenced by enhanced TS conjugation. In addition, localization of a positive charge between the two benzenes shows delocalization TS region. Interestingly, the increase of TB conjugation produces characteristic frequency downshifts of the most intense Raman bands.

In summary, dual fluorescence and Raman shifts provide the fingerprints for TS π-electron delocalization and allows us to comprehensively explore the excited-state and ground electronic-state properties when TB and TS π-electron delocalization compete for the exciton or for the injected charge. Very recently (porphyrin)donor−(fullerene)acceptor molecules connected by distilbenoid pCp units have been described.[5] For these, direct porphyrin → C_{60} electron transfer efficiently occurs by means of the participation of the "phane" state which helps the energy migration and permits final charge separation. However, when this charge separated state structurally relaxes, it is confined to the two disconnected branches because of the absence of "phane" connecting states. This exemplifies the importance of in-depth understanding of the excited-state properties and distribution to design and

DOI: 10.1021/jacs.6b12520
J. Am. Chem. Soc. 2017, 139, 3095−3105

prepare efficient molecular systems for organic electronic applications.

■ ASSOCIATED CONTENT

Supporting Information

The Supporting Information is available free of charge on the ACS Publications website at DOI: 10.1021/jacs.6b12520.

Synthetic procedures, chemical characterizations, details of the quantum chemical calculations (PDF)

■ AUTHOR INFORMATION

Corresponding Authors

*teodomiro@uma.es
*nazmar@ucm.es
*casado@uma.es

ORCID

Miriam Peña-Alvarez: 0000-0001-7056-7158
Marek Samoc: 0000-0002-5404-2455
Francisco J. Ramírez: 0000-0002-8149-9143
Luis Echegoyen: 0000-0003-1107-9423
Nazario Martín: 0000-0002-5355-1477
Juan Casado: 0000-0003-0373-1303

Notes

The authors declare no competing financial interest.

■ ACKNOWLEDGMENTS

The work at the University of Málaga was supported by MINECO through project reference CTQ2012-33733 and by the Junta de Andalucía through research project P09-FQM-4708. The work at the Complutense University of Madrid was supported by European Research Council ERC- 320441 (Chirallcarbon), MINECO of Spain (CTQ2014-52045-R), and Comunidad Autónoma of Madrid (FOTOCARBON project S2013/MIT-2841). T.M.P. acknowledges University of Minnesota, Morris (UMM) Faculty Research Enhancement Funds supported by the University of Minnesota Office of the Vice President for Research. L.E. thanks the Robert A. Welch Foundation, grant AH-0033, and the U.S. National Science Foundation, grants DMR-1205302 and CHE-1408865, for generous financial support. M.S. acknowledges the National Science Centre DEC-2013/10/A/ST4/00114 grant.

■ REFERENCES

(1) Bartholomew, G. P.; Bazan, G. C. *Acc. Chem. Res.* **2001**, *34*, 30−39.
(2) Bazan, G. C.; Oldham, W. J.; Lachicotte, R. J.; Tretiak, S.; Chernyak, V.; Mukamel, S. *J. Am. Chem. Soc.* **1998**, *120*, 9188−9204.
(3) Hong, J. W.; Woo, H. Y.; Liu, B.; Bazan, G. C. *J. Am. Chem. Soc.* **2005**, *127*, 7435−7443.
(4) Mukhopadhyay, S.; Jagtap, S. P.; Coropceanu, V.; Brédas, J. L.; Collard, D. M. *Angew. Chem.* **2012**, *124*, 11797−11800. Elacqua, E.; Bucar, D. K.; Skvortsova, Y.; Baltrusaitis, J.; Geng, M. L.; MacGillivray, L. R. *Org. Lett.* **2009**, *11*, 5106−5109.
(5) (a) Molina-Ontoria, A.; Wielopolski, M.; Gebhardt, J.; Gouloumis, A.; Clark, T.; Guldi, D. M.; Martin, N. *J. Am. Chem. Soc.* **2011**, *133*, 2370−2373. (b) Wielopolski, M.; Molina-Ontoria, A.; Schubert, C.; Margraf, J. T.; Krokos, E.; Kirschner, J.; Gouloumis, A.; Clark, T.; Guldi, D. M.; Martín, M. *J. Am. Chem. Soc.* **2013**, *135*, 10372−10381.
(6) Vogtle, F. *Cyclophane Chemistry*; J. Wiley & Sons: Chichester, England, 1993. *Modern Cyclophane Chemistry*; Gleiter, R., Hopf, H., Eds.; Wiley-VCH: Weinheim, Germany, 2004.
(7) Ruseckas, A.; Namdas, E. B.; Lee, J. Y.; Mukamel, S.; Wang, S.; Bazan, G. C.; Sundstrom, V. *J. Phys. Chem. A* **2003**, *107*, 8029−8034.
(8) Woo, H. Y.; Hong, J. W.; Liu, B.; Mikhailovsky, A.; Korystov, D.; Bazan, G. C. *J. Am. Chem. Soc.* **2005**, *127*, 820−821.
(9) Bartholomew, G. P.; Rumi, M.; Pond, S. J.K.; Perry, J. W.; Tretiak, S.; Bazan, G. C. *J. Am. Chem. Soc.* **2004**, *126*, 11529−11542. Zyss, J.; Ledoux, I.; Volkov, S.; Chernyak, V.; Mukamel, S.; Bartholomew, G. P.; Bazan, G. C. *J. Am. Chem. Soc.* **2000**, *122*, 11956−11962.
(10) Salhi, F.; Lee, B.; Metz, C.; Bottomley, L. A.; Collard, D. M. *Org. Lett.* **2002**, *4*, 3195−3198.
(11) Salhi, F.; Collard, D. M. *Adv. Mater.* **2003**, *15*, 81−85.
(12) Jagtap, S. P.; Mukhopadhyay, S.; Coropceanu, V.; Brizius, G. L.; Brédas, J. L.; Collard, D. M. *J. Am. Chem. Soc.* **2012**, *134*, 7176−7185. Knoblock, K. M.; Silvestri, C. J.; Collard, D. M. *J. Am. Chem. Soc.* **2006**, *128*, 13680−1368.
(13) Canuto, S.; Zerner, M. C. *J. Am. Chem. Soc.* **1990**, *112*, 2114−2120.
(14) Fuke, K.; Nagakura, S.; Kobayashi, T. *Chem. Phys. Lett.* **1975**, *31*, 205−207.
(15) Kaiser, C.; Schmiedel, A.; Holzapfel, M.; Lambert, C. *J. Phys. Chem. C* **2012**, *116*, 15265−15280.
(16) Leng, W.; Grunden, J.; Bartholomew, G. P.; Bazan, G. C.; Myers Kelley, A. *J. Phys. Chem. A* **2004**, *108*, 10050−10059.
(17) Moran, A. M.; Bartholomew, G. P.; Bazan, G. C.; Myers Kelley, A. *J. Phys. Chem. A* **2002**, *106*, 4928−4937.
(18) Nelsen, S. F.; Konradsson, A. E.; Telo, J. P. *J. Am. Chem. Soc.* **2005**, *127*, 920−925.
(19) (a) Ullmann, K.; Coto, P. B.; Leitherer, S.; Molina-Ontoria, A.; Martín, N.; Thoss, M.; Weber, H. B. *Nano Lett.* **2015**, *15*, 3512−3518. (b) Nirmalraj, P.; Thompson, D.; Molina-Ontoria, A.; Sousa, M.; Martín, N.; Gotsmann, B.; Riel, H. *Nat. Mater.* **2014**, *13*, 947−953. (c) Wolfrum, W.; Pinzón, J. R.; Molina-Ontoria, A.; Gouloumis, A.; Martín, N.; Echegoyen, L.; Guldi, D. M. *Chem. Commun.* **2011**, *47*, 2270−2272. (d) Eng, M. P.; Shoaee, S.; Molina-Ontoria, A.; Gouloumis, A.; Martín, N.; Durrant, J. R. *Phys. Chem. Chem. Phys.* **2011**, *13*, 3721−3729.
(20) Szeremeta, J.; Kolkowski, R.; Nyk, M.; Samoc, M. *J. Phys. Chem. C* **2013**, *117*, 26197−26203.
(21) Sheik-bahae, M.; Said, A. A.; Van Stryland, E. W. *Opt. Lett.* **1989**, *14*, 955−957.
(22) Del Corro, E.; González, J.; Taravillo, M.; Flahaut, E.; Baonza, V. G. *Nano Lett.* **2008**, *8*, 2215−2218.
(23) Loubeyre, P.; Occelli, F.; LeToullec, R. *Nature* **2002**, *416*, 613−617.
(24) Baer, B. J.; Chang, M. E.; Evans, W. J. *J. Appl. Phys.* **2008**, *104*, 034504.
(25) (a) Piermarini, G. J.; Block, S.; Barnett, J. D.; Forman, J. A. *J. Appl. Phys.* **1975**, *46*, 2774. (b) Syassen, K. *High Pressure Res.* **2008**, *28*, 75−126.
(26) Baonza, V. G.; Taravillo, M.; Arencibia, A.; Cáceres, M.; Núñez, J. *J. Raman Spectrosc.* **2003**, *34*, 264−270.
(27) Stephens, P. J.; Devlin, F. J.; Chabalowski, C. F.; Frisch, M. J. *J. Phys. Chem.* **1994**, *98*, 11623.
(28) Frisch, M. J.; Trucks, G. W.; Schlegel, H. B.; Scuseria, G. E.; Robb, M. A.; Cheeseman, J. R.; Scalmani, G.; Barone, V.; Mennucci, B.; Petersson, G. A.; Nakatsuji, H.; Caricato, M.; Li, X.; Hratchian, H. P.; Izmaylov, A. F.; Bloino, J.; Zheng, G.; Sonnenberg, J. L.; Hada, M.; Ehara, M.; Toyota, K.; Fukuda, R.; Hasegawa, J.; Ishida, M.; Nakajima, T.; Honda, Y.; Kitao, O.; Nakai, H.; Vreven, T.; Montgomery, J. A., Jr.; Peralta, P. E.; Ogliaro, F.; Bearpark, M.; Heyd, J. J.; Brothers, E.; Kudin, K. N.; Staroverov, V. N.; Kobayashi, R.; Normand, J.; Raghavachari, K.; Rendell, A.; Burant, J. C.; Iyengar, S. S.; Tomasi, J.; Cossi, M.; Rega, N.; Millam, N. J.; Klene, M.; Knox, J. E.; Cross, J. B.; Bakken, V.; Adamo, C.; Jaramillo, J.; Gomperts, R.; Stratmann, R. E.; Yazyev, O.; Austin, A. J.; Cammi, R.; Pomelli, C.; Ochterski, J. W.; Martin, R. L.; Morokuma, K.; Zakrzewski, V. G.; Voth, G. A.; Salvador, P.; Dannenberg, J. J.; Dapprich, S.; Daniels, A. D.; Farkas, Ö.; Ortiz, J.

DOI: 10.1021/jacs.6b12520
J. Am. Chem. Soc. 2017, 139, 3095−3105

V.; Cioslowski, J.; Fox, D. J. *Gaussian 09*, revision A.08; Gaussian, Inc.: Wallingford, CT, 2009.
(29) Becke, A. D. *J. Chem. Phys.* **1993**, *98*, 1372.
(30) Francl, M. M.; Pietro, W. J.; Hehre, W. J.; Binkley, J. S.; Gordon, M. S.; Defrees, D. J.; Pople, J. A. *J. Chem. Phys.* **1982**, *77*, 3654.
(31) Scott, A. P.; Radom, L. *J. Phys. Chem.* **1996**, *100*, 16502.
(32) Grabowski, Z. R.; Rotkiewicz, K.; Rettig, W. *Chem. Rev.* **2003**, *103*, 3899−4032. Sasaki, S.; Drummen, G.P. C.; Konishi, G. *J. Mater. Chem. C* **2016**, *4*, 2731−2743.
(33) Shi, Y.; Frattarelli, D.; Watanabe, N.; Facchetti, A.; Cariati, E.; Righetto, S.; Tordin, E.; Zuccaccia, C.; Macchioni, A.; Wegener, S. L.; Stern, C. L.; Ratner, M. A.; Marks, T. J. *J. Am. Chem. Soc.* **2015**, *137*, 12521−12538. He, G. S.; Zhu, J.; Baev, A.; Samoc, M.; Frattarelli, D. L.; Watanabe, N.; Facchetti, A.; Ågren, H.; Marks, T. J.; Prasad, P. N. *J. Am. Chem. Soc.* **2011**, *133*, 6675−6680.
(34) Li, W.; Sui, Z.; Liu, H.; Zhang, Z.; Liu, H. *J. Phys. Chem. C* **2014**, *118*, 16028−16034.
(35) Samoc, M.; Matczyszyn, K.; Nyk, M.; Olesiak-Banska, J.; Wawrzynczyk, D.; Hanczyc, P.; Szeremeta, J.; Wielgus, M.; Gordel, M.; Mazur, L.; Kolkowski, R.; Straszak, B. M. P.; Humphrey, M. G. *Proceedings of the SPIE: Organic Photonic Materials and Devices XIV*, San Francisco, CA, January 21, 2012; SPIE: Bellingham, WA, 2012; Vol. *8258*.
(36) (a) Castiglioni, C.; Tommasini, M.; Zerbi, G. *Philos. Trans. R. Soc., A* **2004**, *362*, 2425−2459. (b) Hernández, V.; Casado, J.; Ramirez, F. J.; Zotti, G.; Hotta, S.; Navarrete, J. T. L. *J. Chem. Phys.* **1996**, *104*, 9271.
(37) Mayorga Burrezo, P.; Zhu, X.; Zhu, S.-F.; Yan, Q.; López Navarrete, J. T.; Tsuji, H.; Nakamura, E.; Casado, J. *J. Am. Chem. Soc.* **2015**, *137*, 3834−3843.
(38) Kwon, O.; Barlow, S.; Odom, A. A.; Beverina, L.; Thompson, N. J.; Zojer, E.; Bredas, J. L.; Marder, S. R. *J. Phys. Chem. A* **2005**, *109*, 9346−9352.
(39) Bredas, J. L. *J. Chem. Phys.* **1985**, *82*, 3808−3811. Hotta, S.; Waragai, K. *J. Phys. Chem.* **1993**, *97*, 7427−7434.

DOI: 10.1021/jacs.6b12520
J. Am. Chem. Soc. 2017, 139, 3095−3105